# Structure and Dynamics of the Glucocorticoid Receptor DNA-Binding Domain: Comparison of Wild Type and a Mutant with Altered Specificity†

Helena Berglund, Magnus Wolf-Watz, Thomas Lundbäck, Susanne van den Berg, and Torleif Härd*

*Center for Structural Biochemistry, Royal Institute of Technology and Karolinska Institute, Novum, S-141 57 Huddinge, Sweden*

*Received February 14, 1997; Revised Manuscript Received June 9, 1997*⊗

ABSTRACT: Nuclear magnetic resonance was used to compare parameters reflecting solution structure and dynamics of the glucocorticoid receptor DNA-binding domain (GRDBD), which binds specifically to a GRE binding site on DNA, and a triple mutant ($GRDBD_{EGA}$), which binds to an ERE site. The studies were prompted by an earlier observation that the cooperativity for dimeric DNA-binding is 10 times higher for the $GRDBD_{EGA}$−ERE association than for the GRDBD−GRE association (Lundbäck et al., 1994). The higher binding cooperativity of the mutant was unexpected since the triple mutation (G458E, S459G, and V462A) is made in the recognition helix and distant from the dimerization surface which is formed by residues in the fragment A477−N491. Sequential and long-range NOE connectivities and measured $^3J_{HNH\alpha}$ coupling constants indicate that the overall structures of the two proteins are very similar, possibly with a less well-defined structure of the fragment K486−N491 in $GRDBD_{EGA}$. However, chemical shift changes, line broadening, and increased amide proton exchange rates are observed for several residues at, or close to, the dimerization surface of the mutant. These observations are interpreted as a lower stability and/or several slowly interconverting folded conformations of this region of $GRDBD_{EGA}$. The effects are likely to be due to the loss of a hydrogen bond which links S459 to the dimerization region in GRDBD. Different mechanisms for the increased binding cooperativity of the mutant are discussed, and it is noted that the properties of the $GRDBD_{EGA}$ dimerization region are reminiscent of those reported for the estrogen receptor DBD, which also binds to an ERE site.

The glucocorticoid receptor (GR)[1] is a ligand inducible transcription factor which belongs to the nuclear receptor superfamily. All members of this superfamily contain a highly conserved DNA-binding domain (DBD, Figure 1a) which is necessary, and by itself sufficient, for sequence specific DNA binding (Freedman et al., 1988). Two GRDBD monomers bind cooperatively to glucocorticoid DNA response elements (GREs). The consensus GRE is composed of two palindromically arranged hexameric half-sites, separated by an intervening sequence of three base pairs (Figure 1b). Several structural studies have been carried out, both of the uncomplexed GRDBD in solution (Härd et al., 1990, Baumann et al., 1993, van Tilborg et al., 1995) and of crystals of the dimeric GRDBD−DNA complex (Luisi et al., 1991). Structural data are also available on the closely related estrogen receptor DNA-binding domain (ERDBD), free in solution and in complex with DNA (Schwabe et al., 1990, 1993, 1995) as well as on mutated forms of GRDBD in complex with DNA (Xu et al., 1993, Gewirth & Sigler, 1995).

Three amino acids, G458, S459, and V462, together named the P-box (Figure 1a), are situated in the recognition helix of GRDBD and are responsible for discrimination between a GRE and an estrogen receptor response element (ERE). ERE and GRE differ in two base pairs in the centre of each half-site (Figure 1b). Mutation of the three P-box residues to the corresponding amino acids in the estrogen receptor DNA binding domain (ERDBD) (i.e., G458E, S459G, V462A) switches the specificity of the mutant $GRDBD_{EGA}$ from GRE specificity to ERE specificity (Danielsen et al., 1989; Umesono & Evans, 1989; Zilliacus et al., 1991). The functions of the P-box residues have been studied in terms of DNA-binding specificity of single, double, and triple P-box mutants (Zilliacus et al., 1991). In GRDBD V462 makes a hydrophobic contact with the methyl group of the GRE-specific thymine at position 3 in GRE and appears also to contribute negatively to binding to ERE. In the same way, a glutamate in ERDBD, corresponding to G458 in GRDBD, forms a hydrogen bond with the ERE-specific cytosine at position 4 but provides a negative steric contribution to GRE-binding. S459, on the other hand, is not involved in any direct base contact but reduces the affinity for both response elements, although with a larger negative effect for ERE-binding than for GRE-binding (Zilliacus et al., 1992). In the GRDBD−GRE complex, there is a hydrogen bond between the hydroxyl oxygen of S459 and an $N^{\eta}H_2$ of R489 in the C-terminal zinc-coordinating domain (Figure 2). The importance of this hydrogen bond for the inhibitory action in ERE-binding is supported by the observation that an EAA P-box mutant, in which the hydroxyl and thereby the hydrogen bond acceptor is removed, preferably binds to a GRE but also can bind to an ERE. On the other hand, the P-box mutations ESA, ETA, and ECA, all with a potential hydrogen bond acceptor in the side chain of the residue at position 459, do not allow binding to an ERE (Zilliacus et

† This work was supported by a grant from the Swedish Natural Sciences Research Council.

⊗ Abstract published in *Advance ACS Abstracts,* August 15, 1997.

[1] Abbreviations: GR, glucocorticoid receptor; GRDBD, glucocorticoid receptor DNA-binding domain; ERDBD, estrogen receptor DNA-binding domain; GRE, glucocorticoid response element; ERE, estrogen response element; NMR, nuclear magnetic resonance; NOE, nuclear Overhauser enhancement; NOESY, NOE spectroscopy; TOCSY, total correlation spectroscopy; HSQC, heteronuclear single-quantum correlation; DTT, dithiothreitol.

S0006-2960(97)00343-7 CCC: $14.00 

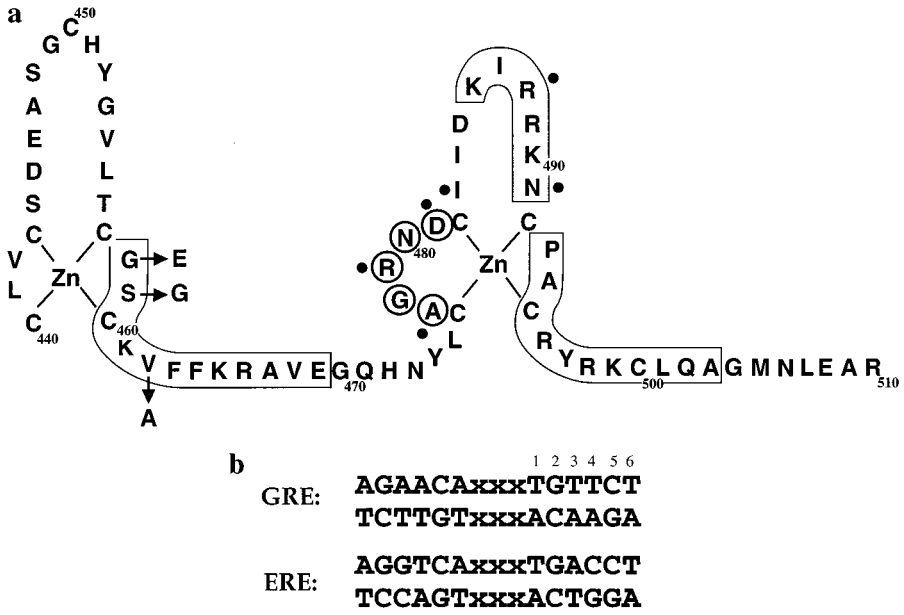


FIGURE 1: (a) Amino acid sequence of the glucocorticoid receptor DNA-binding domain (GRDBD) with the P-box mutations yielding $GRDBD_{EGA}$ indicated with arrows. D-box residues are shown in circles and residues making protein−protein contacts in the dimeric DNA complex (Luisi et al., 1991) are indicated with solid dots. The boxes correspond to helical regions in the wild type protein (K486−N491 is not a classical α-helix). (b) Consensus sequences of the glucocorticoid response element (GRE) and the estrogen response element (ERE).

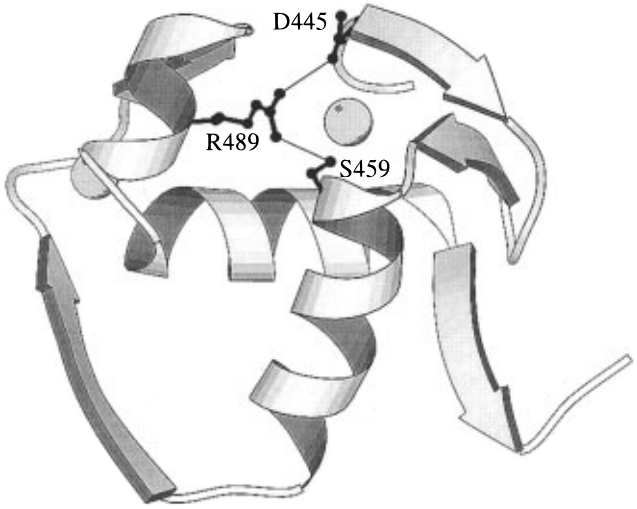


FIGURE 2: The hydrogen bonding network R489−D445 and R489−S459, which links the two zinc-coordination subdomains, is shown in a Molscript picture (Kraulis, 1991) of one monomer from the crystal structure of the GRDBD−GRE complex (Luisi et al., 1991).

al., 1994). Still, the molecular mechanism by which the residue in position 459 exerts its function remains obscure.

In a previous study we examined the DNA-binding properties of the $GRDBD_{EGA}$ triple mutant (Lundbäck et al., 1994). The most noticeable difference between the dimeric GRDBD−GRE and $GRDBD_{EGA}$−ERE binding processes is the considerably larger binding cooperativity displayed by the mutant. Cooperative DNA-binding depends on protein−protein interactions in the second zinc-coordinating subdomain (Figure 1a) (Dahlman-Wright et al., 1990, 1991) and the structure of this region appears to differ depending on the protein studied as well as if it is free in solution or bound to DNA. In uncomplexed GRDBD, the structure of this segment resembles that in the DNA-bound form (Baumann et al., 1993), but in the uncomplexed ERDBD, this peptide segment is poorly defined (Schwabe et al., 1990). Also in the crystal structures of ERDBD complexed with DNA, different conformations of this region are seen (Schwabe et al., 1993, 1995). Initial NMR studies of $GRDBD_{EGA}$, which preferentially binds to an ERE, revealed chemical shift differences and some broadened amide proton resonances in the second zinc-coordinating domain, distant from the site of mutation. These observations prompted the question of whether preferential binding to an ERE and/or increased cooperativity of binding is connected to increased flexibility of the dimerization domain and motivated us to further characterize the effects of the triple mutation on structure and dynamics.

## MATERIALS AND METHODS

### *NMR Sample Preparation*

$^{15}N$-labeled wild type GRDBD (K438−Q520 of the rat GR) and triple-mutant $GRDBD_{EGA}$ (Zilliacus et al., 1991) were overproduced in *Escherichia coli* strain BL21(DE3)-pLysS using the pT7-7 overexpression system. Cells were grown at 37 °C in a minimal medium containing 0.5 g of $^{15}NH_4Cl$, 3 g of $KH_2PO_4$, 1.2 g of $Na_2HPO_4$, 0.25 g of NaCl, 1 g of sodium citrate, 0.24 g of $MgSO_4$, 0.5% glucose, 13.6 mg of $ZnCl_2$, trace amounts of $Na_2MoO_4$, $CaCl_2$, and $H_3BO_3$, and 0.1% Isogro-$^{15}N$ powder growth medium (Isotec Inc) per liter of medium. When the absorbance at 600 nm reached 0.6, protein expression was induced by addition of 0.2 mM isopropyl β-D-thiogalactopyranoside (IPTG) and cells were harvested after 2 h. The cells were lysed in a buffer containing 500 mM NaCl, 50 mM Tris, 1 mM EDTA, 1 mM $ZnCl_2$, 10% glycerol, 5 mM DTT, 0.05% deoxycholic acid, and protease inhibitors at pH 7.5 using a French Press (SLM Instruments Inc.), and the cell extract was cleared by centrifugation. DNA was preciptitated by addition of 0.2% polyethylenimine and removed by centrifugation. Following precipitation of the protein fraction by addition of 70% $(NH_4)_2SO_4$, the pellet was resuspended and dialyzed against 50 mM Tris, 1 mM EDTA, 50 mM NaCl, 0.1 mM $ZnCl_2$, and 1 mM DTT at pH 8.0. The dialyzed material was loaded on a CM-Sepharose (Pharmacia) ion exchange column, washed with 100 mM NaCl, 20 mM $NaH_2PO_4$, and 1 mM

DTT at pH 7.6 and eluted with a linear salt gradient to 800 mM NaCl. The collected fractions were further purified using a Pharmacia Superdex 75 16/60 gel-filtration column in the NMR buffer (150 mM NaCl, 20 mM $NaH_2PO_4$ and 2 mM DTT at pH 6.0). Following concentration of NMR samples in Centricon-3 concentrators (Amicon), the pH was adjusted to 6.0. NMR tubes containing sample were repeatedly flushed with nitrogen before closure to minimize the amount of dissolved oxygen.

*NMR Spectroscopy*

NMR spectra were recorded at 26 and 30 °C on a Varian Unity 500 MHz spectrometer using a 5 mm triple-resonance ($^1H/^{13}C/^{15}N$) pulsed field gradient probe. Varian Software (VNMR 4.3) was used for data processing. For quantitative analyses described below, intensities were measured as peak heights and uncertainties were estimated on the basis of the measured peak height to base line noise ratios.

The reference chemical shifts of GRDBD are those reported by Baumann et al. (1993, Supporting Information) with the exception of $^{15}N_{N475}$ and $^{15}N_{N491}$ which have been re-assigned to 126.7 and 118.7 ppm, respectively (H. Baumann, unpublished). For assignment of $GRDBD_{EGA}$ resonances we recorded a two-dimensional clean TOCSY (Griesinger et al., 1988) spectrum with a 70 ms isotropic mixing time, a 2D NOESY spectrum (Macura & Ernst, 1980) with a cross-relaxation mixing time of 150 ms, as well as 3D $^{15}N$-edited NOESY-HSQC and TOCSY-HSQC spectra. The 3D experiments were implemented as combinations (Gronenborn et al., 1989) of NOESY and clean TOCSY with gradient-selected HSQC (Davis et al., 1992). $GRDBD_{EGA}$ resonances were assigned using conventional methods utilizing the interactive graphics program ANSIG v. 3.2 (Kraulis, 1989). $^1H$ shifts are referenced to $H_2O$ at 4.74 ppm at 26 °C and $^{15}N$ chemical shifts to external [$^{15}N$]benzamide at 105.4 ppm as are those of the wild type GRDBD (Baumann et al., 1993).

Differences in amide proton exchange rates between GRDBD and $GRDBD_{EGA}$ were estimated on the basis of measurements of magnetization transfer following saturation of the water resonance. The saturation transfer (Forsén & Hoffman, 1963) measurements were performed as gradient selected $^1H-^{15}N$ HSQC (Davis et al. 1992) experiments recorded with and without selective presaturation of the water with a field strength of 24 Hz during 1 s. Assuming an amide proton relaxation time $T_{1,HN} = 0.2$ s for a protein corresponding to the size of GRDBD (Spera et al., 1991; Peng & Wagner, 1992) one can expect steady-state conditions to apply and the exchange rate $k_{ex}$ is given by [$k_{ex} = (1 - I/I_o)/T_{1,HN}$]. For the present analysis we adopt the Linderstrøm−Lang model for the exchange mechanism (Hvidt & Nielsen, 1966), in which $k_{open}$ and $k_{close}$ are the rates for (local or global) unfolding and folding reactions, respectively, and $k_{intrinsic}$ is the intrinsic rate of exchange for a specific residue in an exposed (open) state under certain pH and temperature conditions. Considering the rapid exchange of GRDBD amide protons and the present pH and temperature conditions one may assume EX2 behavior, i.e., $k_{ex} = (k_{open}/k_{close})k_{intrinsic}$ (Hvidt & Nielsen, 1966). Following Englander and Kallenbach (1984) the exchange rate can be related to the free energy difference $\Delta G$ between the open and closed states as $\Delta G = -RT \ln(k_{ex}/k_{intrinsic})$. Differences in $\Delta G$ values (of nonmutated residues) between wild type and mutant protein can then be estimated directly from measured intensities as

$$\delta\Delta G = -RT \ln(k_{ex,mut}/k_{ex,wt}) = -RT \ln((1 - I/I_o)_{mut}/(1 - I/I_o)_{wt}) \quad (1)$$

3D HNHA (Kuboniwa et al., 1994) spectra for measurement of vicinal $^3J_{HNH\alpha}$ coupling constants were recorded on both proteins using a rephasing period ($\xi$) of 13 ms. $^3J_{HNH\alpha}$ coupling constants were calculated from intensities measured as peak heights using the expression [$I_{crosspeak}/I_{diagonal} = -\tan^2(2\pi\xi\ ^3J_{HNH\alpha})$]. The small correction factor compensating for the reduction in measured $^3J_{HNH\alpha}$ values due to $^1H-^1H$ cross relaxation (Kuboniwa et al., 1994) was not applied, since the objective was to make qualitative comparisons of wild type and mutant proteins with almost identical molecular weights.

$\{^1H\}-^{15}N$ steady state NOEs and $^{15}N$ $T_2$ relaxation times in $GRDBD_{EGA}$ were measured using pulse sequences described by Farrow et al. (1994, Figure 10b,c), kindly provided by Dr. L. E. Kay (University of Toronto). These experiments employ sensitivity enhancement based on gradient selection. Steady state NOEs are defined as the ratio $I_{sat}/I_o$ where $I_{sat}$ and $I_o$ are measured in spectra recorded with and without $^1H$ saturation, respectively. Proton saturation was achieved by application of 120° pulses spaced at 5 ms intervals for 3 s, and the total delay between scans was 5 s. In the $T_2$ measurements, cross-correlation between $^1H-^{15}N$ dipolar and $^{15}N$ chemical shift anisotropy relaxation mechanisms is eliminated by the insertion of $^1H$ 180° pulses during the relaxation time. The CPMG refocusing delay $\delta$ was set to 450 $\mu$s, and relaxation delays of 0.062, 0.094, 0.125, 0.156, 0.189, 0.219, 0.250, and 0.281 s were used. $T_2$ relaxation times were obtained from fits of the intensities to a single exponential.

## RESULTS

To obtain a first indication of where in the protein changes might have occurred as a consequence of the mutation, we compared the chemical shifts of the amide nitrogen (N), amide proton (HN), and α-proton (Hα) resonances in the $GRDBD_{EGA}$ mutant with the corresponding chemical shifts in GRDBD taken from (Baumann et al. (1993) (Figure 3). Most resonances stay unaffected by the mutation, i.e., they differ less than the average line width of 0.08 and 1.4 ppm in $^1H$ and $^{15}N$ dimensions, respectively. However, apart from differences in the direct vicinity of the mutated residues, significantly different chemical shifts are observed in a region distant from the site of mutation. Residues A477, and G478 in the N terminus of the second zinc-coordinating domain (Figure 1a), experience shift changes in their backbone nitrogen or amide proton resonances. More pronounced differences are found further toward the C-terminal, where $I484_{H\alpha}$, $D485_{HN,H\alpha}$, $I487_{HN}$, $R488_{HN}$, $K490_{HN,H\alpha}$, $N491_{H\alpha}$, and $C492_{N,HN}$ chemical shifts are affected. The α-proton resonances of A494, C495, and Y497 in the beginning of the third helix (Figure 1a) are also shifted in $GRDBD_{EGA}$ compared to the wild type protein. There is no concentration dependence in the amide $^{15}N$ or $^1H$ chemical shifts in the concentration interval 100 $\mu$M to 2 mM (data not shown), indicating that the observed differences are not an effect of protein dimerization in solution.

Identification of short- and medium-range NOEs in the mutant $GRDBD_{EGA}$ show NOE connectivity patterns that

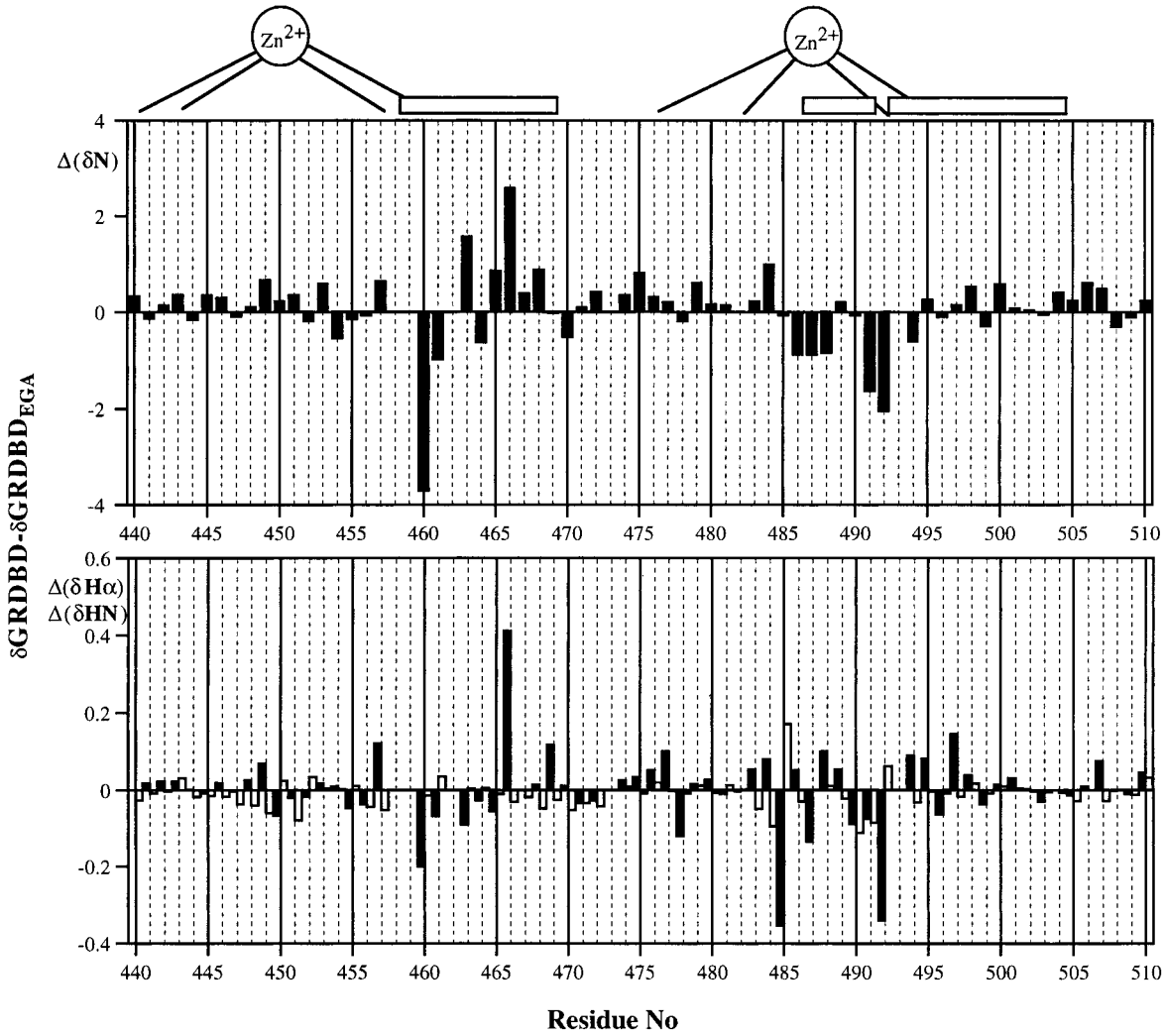


FIGURE 3: Chemical shift differences between GRDBD and $GRDBD_{EGA}$ NMR resonances [$\delta$(GRDBD) − $\delta$($GRDBD_{EGA}$)]. (Top) Backbone nitrogen shifts; (bottom) amide proton (open bars) and α-proton (filled bars) chemical shifts. Secondary structure elements and zinc ion coordination are indicated at the top of the graph.

closly resemble those of the wild type protein (Figure 4). However, some $d_{NN}$ connectivities in the second zinc-coordinating domain are missing, possibly due to exchange broadening of the corresponding amide resonances. Furthermore, NOE connectivities such as $d_{\alpha N}(i,i+2)$ and $d_{\alpha N}(i,i+3)$, defining the distorted helix comprising residues K486−N491, are absent in the mutant. Several identical long-range NOEs, reflecting the overall protein fold, are found in the two proteins.

The value of the $^3J_{HNH\alpha}$ coupling constant depends on the backbone $\phi$ dihedral angle and is thereby a sensitive probe of the peptide backbone conformation. We have measured and compared $^3J_{HNH\alpha}$ coupling constants for the wild type and mutant proteins (Figure 5). Only one residue, I487, shows a difference in $^3J_{HNH\alpha}$ which exeeds the experimental uncertainty, whereas all other residues for which data could be obtained in both proteins show very similar $^3J_{HNH\alpha}$ values.

Several amide proton resonances appear to be attenuated and/or broadened in $GRDBD_{EGA}$ compared to GRDBD. The effect involves residues in the second zinc-coordinating domain, i.e., C482−D485 and C492, as illustrated in HSQC spectra in Figure 6. A direct comparison of lineshapes for the well-resolved resonances shows broadening as well as attenuation of intensity in the mutant. This effect on the amide resonances might arise from increased solvent exchange rates, possibly in combination with an additional slow dynamic process in this region of the protein. We therefore investigated possible differences in the internal dynamics of GRDBD and $GRDBD_{EGA}$ using amide proton exchange measurements and $^{15}N$ relaxation experiments. The two methods complement each other since the $^{15}N$ relaxation is sensitive to fast motions on a picosecond to nanosecond time scale, whereas amide proton exchange rates reflect slower processes. Attempts to quantitate amide proton exchange rates in GRDBD using classical exchange-out experiments show that nearly all amide protons exchange when lyophilized protein is dissolved in $D_2O$ (T. Härd, unpublished). This result suggests that the folding stability of GRDBD in solution and/or in the lyophilized state is low. HSQC spectra recorded with water presaturation show a significant attenuation of most amide proton resonance intensities (not shown). This observation supports the inference of rapid exchange throughout the GRDBD and suggests that comparisons of exchange rates based on saturation transfer measurements (Forsén & Hoffman, 1963) should be more appropriate.

In Figure 7 we compare resonance intensities in HSQC spectra of the wild type and mutant proteins recorded with and without presaturation of the water. The comparison indicates exchange rate differences in the N-terminal region where the exchange appears somewhat slower in the mutant than in the wild type. The slower exchange rate for C460 can be explained by the proximity to the mutation S459G,

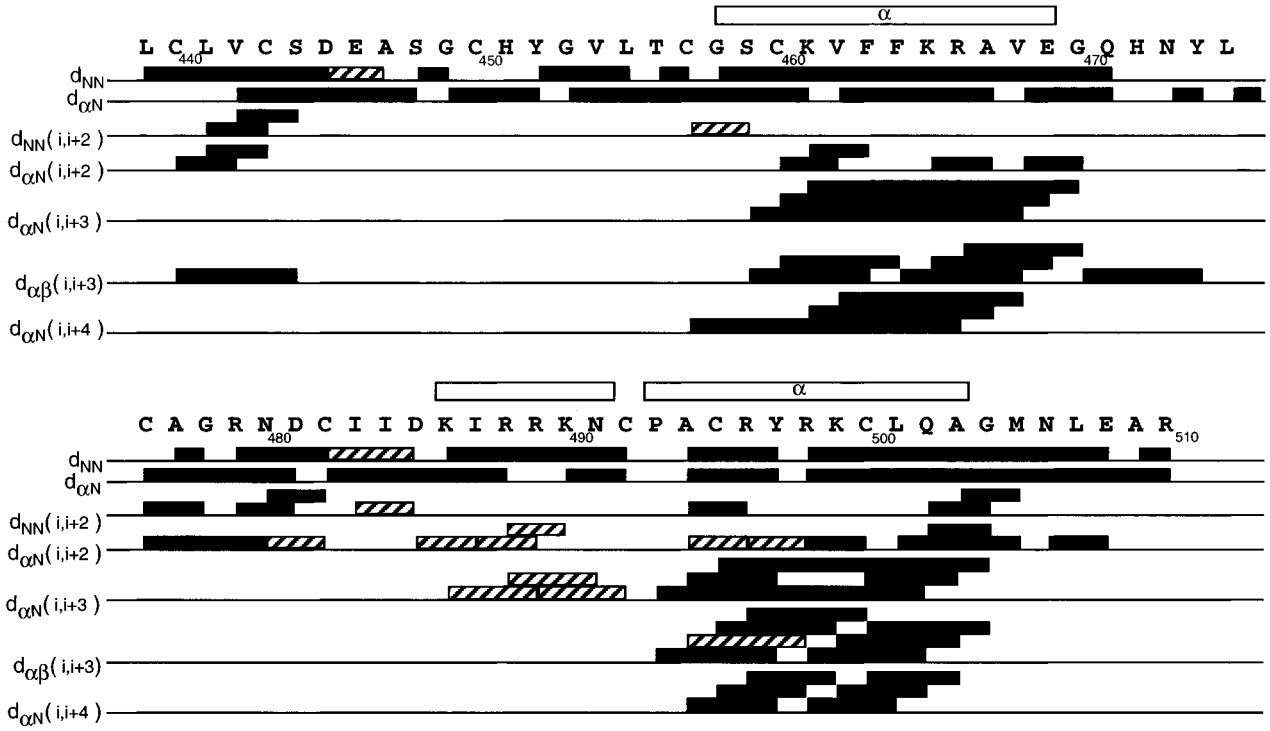


FIGURE 4: Short- and medium-range NOEs in GRDBD (Baumann et al., 1993). NOE connectivities that can be observed in GRDBD but not in $GRDBD_{EGA}$ are shown with striped bars.

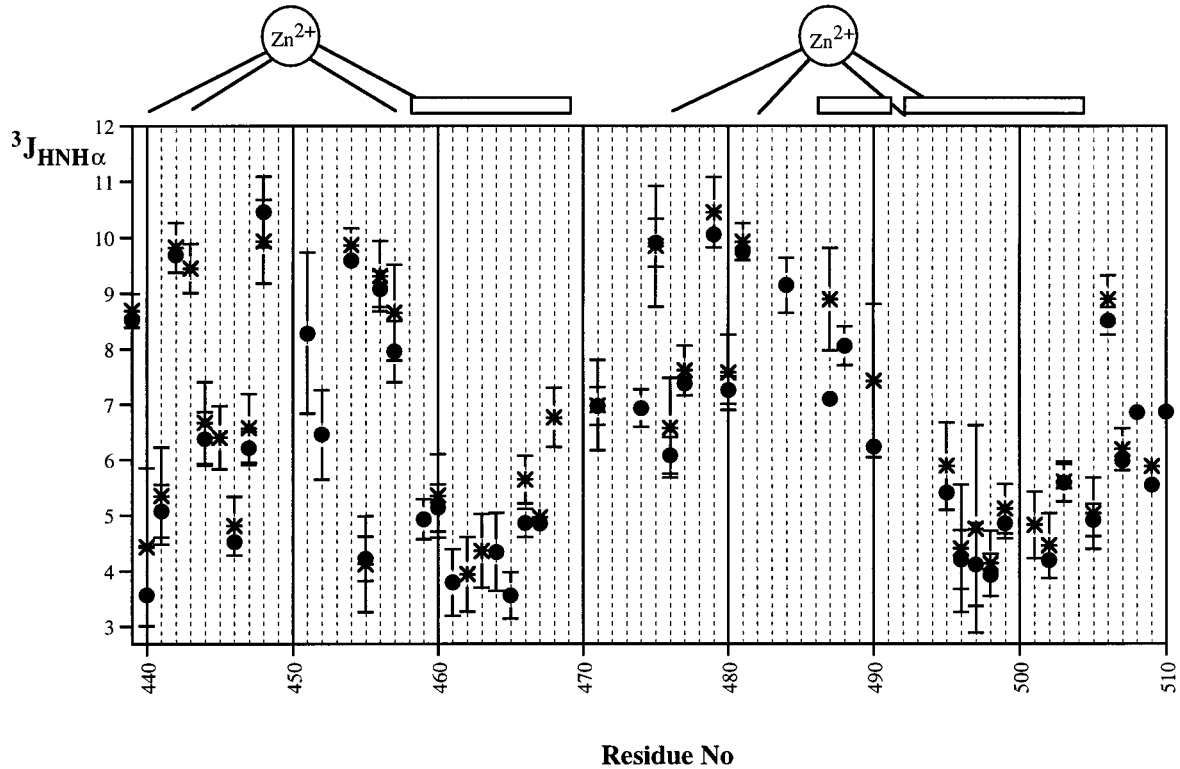


FIGURE 5: Measured $^3J_{HNH\alpha}$ coupling constants in GRDBD (●) and $GRDBD_{EGA}$ (∗).

as neighboring side-chains are important determinants for the amide proton exchange (Bai et al., 1993). For several resonances in the second zinc-coordinating domain, especially I483, D485, K490, and C492, exchange is more rapid in the mutant. In the case of saturation transfer measurements care must be taken not to misinterpret effects that are due to cross-relaxation rather than to exchange. Residues with amide protons that have NOEs to protons resonating close to (<125 Hz from) the water (including D485) in one of the proteins are therefore marked in Figure 7. Equation 1 allows for a quantitative comparison of local stability without explicit calculation of the exchange rates in the mutant and wild type proteins. In terms of $\delta\Delta G$, the residues mentioned above show $\delta\Delta G > 0.15$ kcal/mol with a maximum $\delta\Delta G \approx 0.5$ kcal/mol for I483.

The extent of fast backbone dynamics in GRDBD has previously been investigated by means of $^{15}N$ relaxation experiments, and it was found to be limited and rather uniform throughout the peptide backbone (Berglund et al., 1992). We now measured $\{^1H\}-^{15}N$ steady state NOEs and

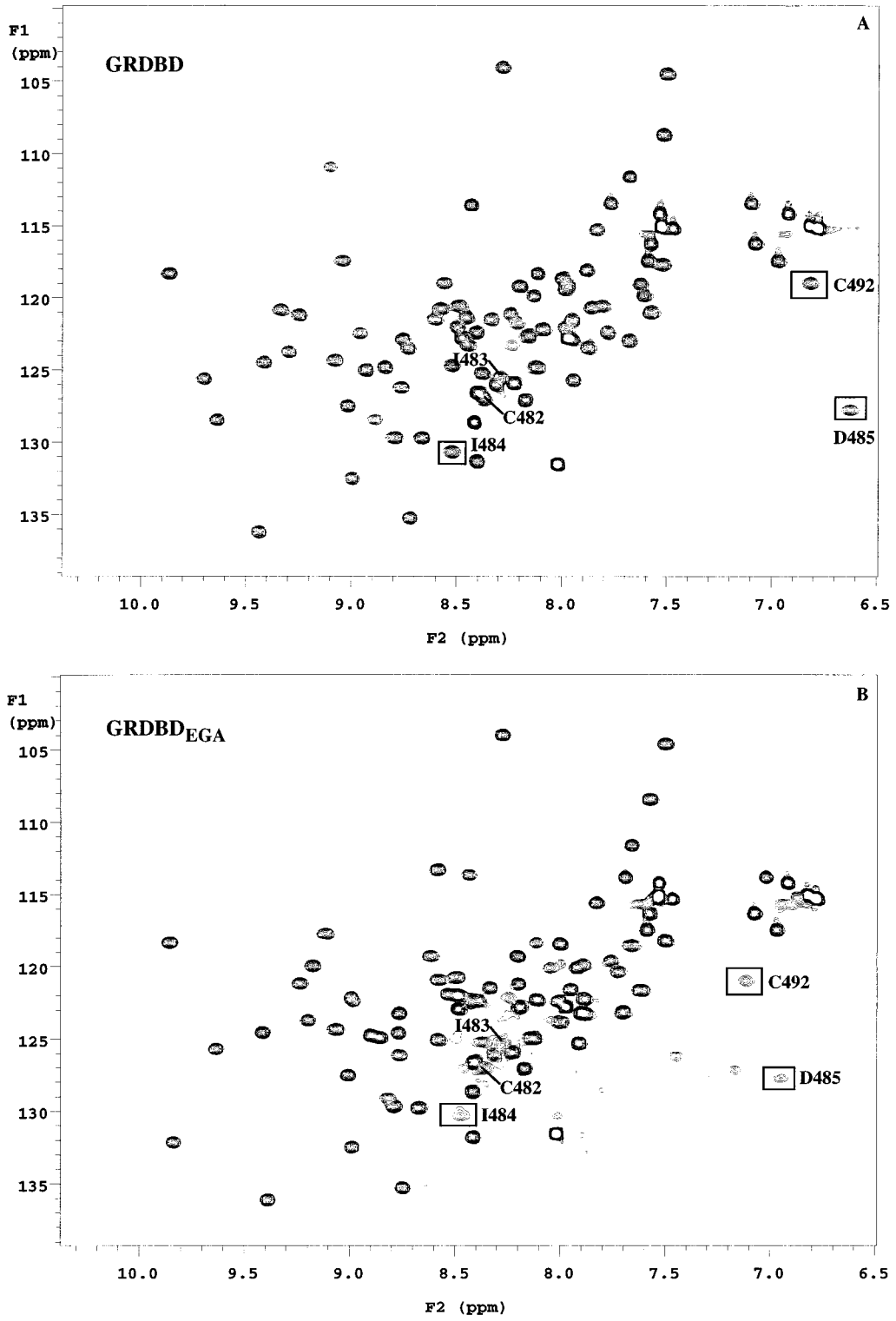


FIGURE 6: $^{1}H-^{15}N$ gradient-selected HSQC spectra of (A) GRDBD and (B) GRDBD$_{EGA}$ recorded at 30 °C. Marked resonances are attenuated and/or broadened in the spectrum of the mutant.

$^{15}N$ $T_2$ relaxation times in GRDBD$_{EGA}$ to identify possible disordered peptide regions in the mutant and to compare the rapid backbone dynamics of the two proteins. Since $^{15}N$ $T_2$ relaxation times also include a contribution from slower dynamic processes, they were particularly interesting to compare in this case. Unfortunately, data for the broadened residues could not be reliably evaluated due to the exchange broadening combined with overlap, but for the other residues similar $T_2$ relaxation times are obtained in the wild type and the mutant (data not shown). Similarly, the (more sensitive) $\{^{1}H\}-^{15}N$ NOE measurement does not indicate any significant differences in picosecond backbone dynamics between the two proteins (Figure 8) with a possible exception of the tip of the finger in the first zinc-coordinating domain, where S448 and G449 have clearly lower NOE values in GRDBD compared to GRDBD$_{EGA}$.

## DISCUSSION

We previously examined the DNA-binding properties of GRDBD$_{EGA}$ (Lundbäck et al., 1994). One notable result was that, although the binding affinity of GRDBD$_{EGA}$ for a response element containing a single ERE half-site is clearly

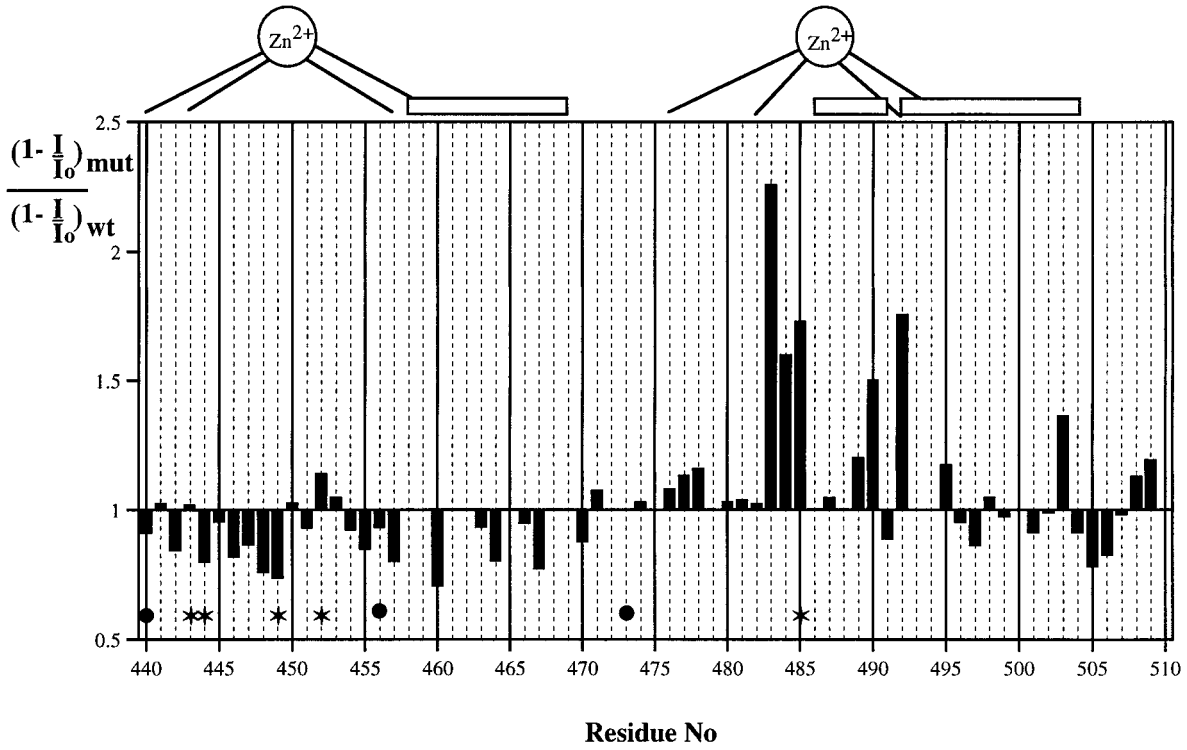


FIGURE 7: Differences in amide proton exchange rates between GRDBD and $GRDBD_{EGA}$ illustrated as $(1 - I_{sat}/I_o)_{mutant}/(1 - I_{sat}/I_o)_{wild\ type}$. Residues in which the amide proton has a direct NOE to a proton resonating close to water in one of the two proteins, are indicated as "●" (only in GRDBD) and "∗" (only in $GRDBD_{EGA}$). A more rapid exchange in $GRDBD_{EGA}$ gives values greater than 1.0 and vice versa.

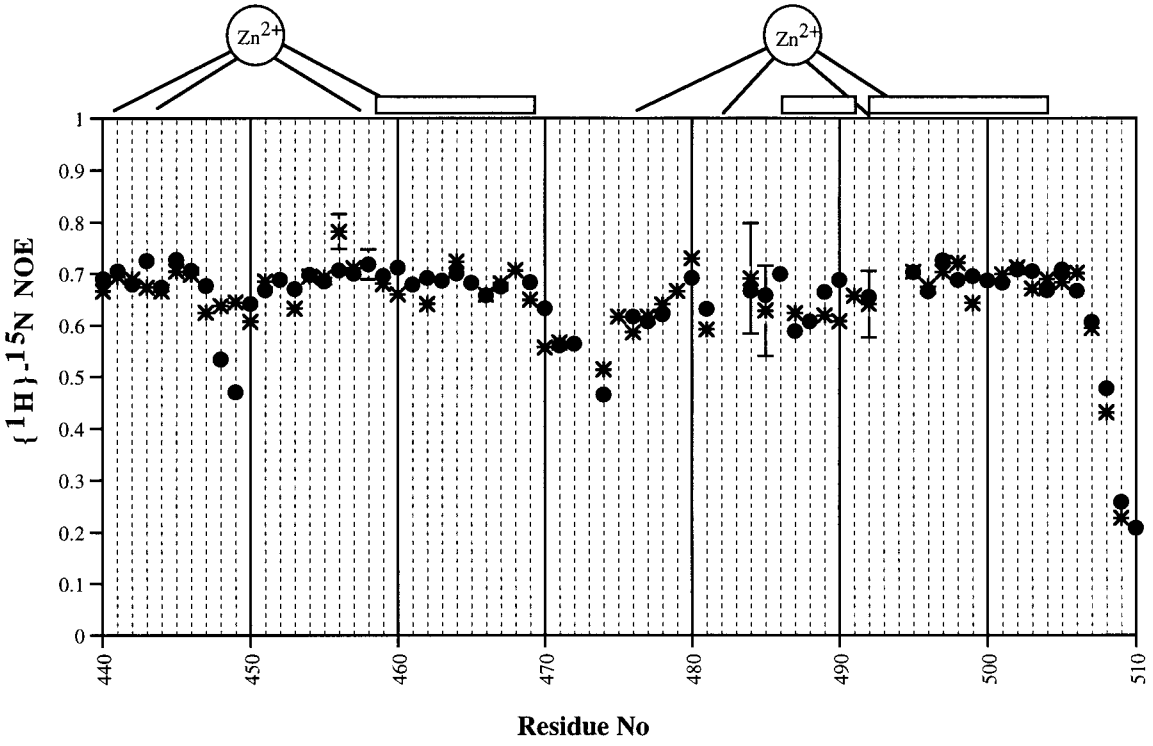


FIGURE 8: Measured $\{^1H\}-^{15}N$ steady state NOEs for GRDBD (●) and $GRDBD_{EGA}$ (∗) where lower values indicate increased mobility on a picosecond to nanosecond time scale.

lower than the binding of one GRDBD monomer to a half-site GRE, the overall affinity of two $GRDBD_{EGA}$ molecules for ERE is similar to the affinity of two GRDBDs for GRE. Obviously, the two binding processes differ significantly in binding cooperativity, and the cooperativity factor, $\omega$, was found to be ten times higher for the $GRDBD_{EGA}$−ERE association compared to the GRDBD−GRE binding.

In this study we have analyzed NMR-parameters sensitive to structure and dynamics in the $GRDBD_{EGA}$ mutant and compared with data on the wild type GRDBD. Chemical shift differences are found not only in the direct surrounding of the triple mutation, but also in the second zinc-coordinating subdomain, distant from the site of mutation both in sequence and structure. Comparison of sequential and

medium range NOE connectivity patterns suggest a similar secondary structure content in the two proteins. However, differences are found in the second zinc-coordinating subdomain where the mutant lacks a few side chain to backbone NOEs that are present in the wild type. With regard to the overall structure, several identical long-range NOEs, indicative of similar global folds, are found in the two proteins. In addition, measured values of $^3J_{HNH\alpha}$ coupling constants compare well between GRDBD and $GRDBD_{EGA}$ and support similar backbone conformations. Taken together, our data is consistent with in essence identical structures of the two proteins, possibly with a less well-defined structure of K486−N491 in the mutant.

A distinction can be made between GRDBD and [$GRDBD_{EGA}$] on basis of the dynamical behavior. $^{15}N$ relaxation experiments, sensitive to protein motions on a short time scale, show little difference between the two proteins. However, in the first zinc-coordinating domain two residues have clearly lower $\{^1H\}-^{15}N$ NOEs and also higher amide hydrogen exchange rates in GRDBD, indicative of a increased mobility in this region compared to the mutant. In the second zinc-coordinating domain, a number of amide proton resonances are broadened in spectra of $GRDBD_{EGA}$. Together with increased exchange rates, this suggests the presence of a slow dynamical process or alternatively, a lower structural stability in this region of the mutant.

The NMR parameters for the second zinc-coordinating subdomain of $GRDBD_{EGA}$ are reminiscent of those of the D-helix in the *trp* aporepressor. The amide proton exchange rates in this helix are higher than those of the stably folded core (Gryk et al., 1995) and most side chain to backbone NOE connectivities signifying a stable helix are not observed (Zhao et al., 1993). One the other hand, $^{15}N$ chemical shift and relaxation data (Zheng et al., 1995) demonstrate that the D-helix peptide fragment predominantly occupies folded conformations. It was in this case concluded that the increased exchange rates and missing NOEs are consequences of many interconverting folded states (Gryk et al., 1995).

Most detected changes between GRDBD and $GRDBD_{EGA}$ proteins in the uncomplexed state are located to the second zinc-coordinating domain as illustrated in Figure 9a,b. Effects occuring distant from the site of mutation can be explained by an altering of the hydrogen bonding possibilities caused by the mutation. In the dimeric GRDBD−GRE complex (Luisi et al., 1991), one of the P-box residues, S459, is involved in a hydrogen bond network also comprising D445 and R489, as illustrated in Figure 2. The network serves as a link between the two subdomains of the protein. In $GRDBD_{EGA}$, S459 is replaced by a glycine, resulting in loss of a hydrogen bond acceptor and, in particular, loss of the potential hydrogen bond between S459 and R489. This hydrogen bond network was not detected in the solution structure of the uncomplexed GRDBD (Baumann et al., 1993), because the involved side chains are located on the surface of the protein and not very well defined in the ensemble of NMR structures. However, it cannot be exluded that the hydrogen bonds are present in the uncomplexed wild type protein, at least part of the time.

In the GRDBD−DNA complex (Luisi et al., 1991), the second zinc-coordinating domain is responsible for several DNA phosphate contacts as well as for the dimeric protein−protein interactions. Differences in the structure and/or dynamics of the C482−C492 fragment and the corresponding region in ERDBD have been discussed. In GRDBD, the structure of this region resembles the DNA-bound form but in ERDBD, in which the residue corresponding to S459 in GR is a glycine and thus the possibility of a hydrogen bond to the arginine corresponding to R489 is missing, this segment appears to be less well-defined as judged from a lack of long-range distance restraints and absence of some amide proton resonances in spectra recorded at high temperatures (Schwabe et al., 1990). Also in the crystal structure of the ERDBD−ERE complex (Schwabe et al., 1993), this region adopts different folds. In GRDBD the five-residue loop between C476 and C482 in the N-terminal of the second zinc-coordinating domain, the D-box (Figure 1a), has been shown to be important for cooperative DNA-binding (Dahlman-Wright et al., 1991). Structurally, the D-box forms part of the dimerization interface and it appears to undergo a modest conformational change upon DNA binding (Baumann et al., 1993).

The dimeric interface in the $GRDBD_{EGA}$−ERE complex has been reported as identical to the one seen in the GRDBD−GRE structure (Xu et al., 1993), i.e., no additional dimeric contacts that could explain the higher cooperativity for the mutant are seen in the structure. It is therefore possible that the increased cooperativity in $GRDBD_{EGA}$ when bound to ERE instead can be related to the stability of the C-terminal subdomain and its ability to form an optimal dimerization surface in the DNA-bound form. If a conformational change, for example reorientation of the D-box loop (Baumann et al., 1993), is necessary for cooperative DNA-binding, a certain structural flexibility in the uncomplexed state could lower the energetic cost of the conformational transition upon binding.

Another explanation for the increased cooperativy in the $GRDBD_{EGA}$ mutant might emanate from DNA. Complexed forms of the two DNA binding sites, GRE and ERE, are similar but not identical in structure and the available structures of different GR/ERDBD-related DNA complexes show that the disposition of the protein on DNA is dependent on the DNA sequence (Luisi et al., 1991; Gewirth & Sigler, 1995; Schwabe et al., 1993, 1995). If the protein monomers adopt slightly different orientations with respect to each other when bound to their corresponding DNA sites, then the difference can be propagated to the dimerization interface and influence the formation hereof. Since the high cooperativity is only manifested when the mutant is bound to ERE but not to GRE (Lundbäck et al., 1994), the positioning of $GRDBD_{EGA}$ on ERE might be the origin of the enhanced cooperativity.

Similar to ERDBD, the $GRDBD_{EGA}$ mutant shows a lower structural stability in the C-terminal zinc-coordinating subdomain, although the effect appears less pronounced in $GRDBD_{EGA}$. The altered stability might be the result of the removal of a stabilizing hydrogen bond which is present in GRDBD but missing in ERDBD. While the ERDBD is unable to bind to a glucocorticoid response element and vice versa (Mader et al., 1989; Zilliacus et al., 1992), our mutant shows a DNA-binding behavior in between the two wild type proteins: $GRDBD_{EGA}$ prefers binding to ERE but still retains some affinity for GRE (Zilliacus et al., 1992). Interestingly, also in structure and dynamics the mutant seems to be intermediate to the two wild type DBDs. A detailed quantitative study of the thermodynamics of the ERDBD−DNA binding process, together with investigations of the internal dynamics of the uncomplexed ERDBD could pos-

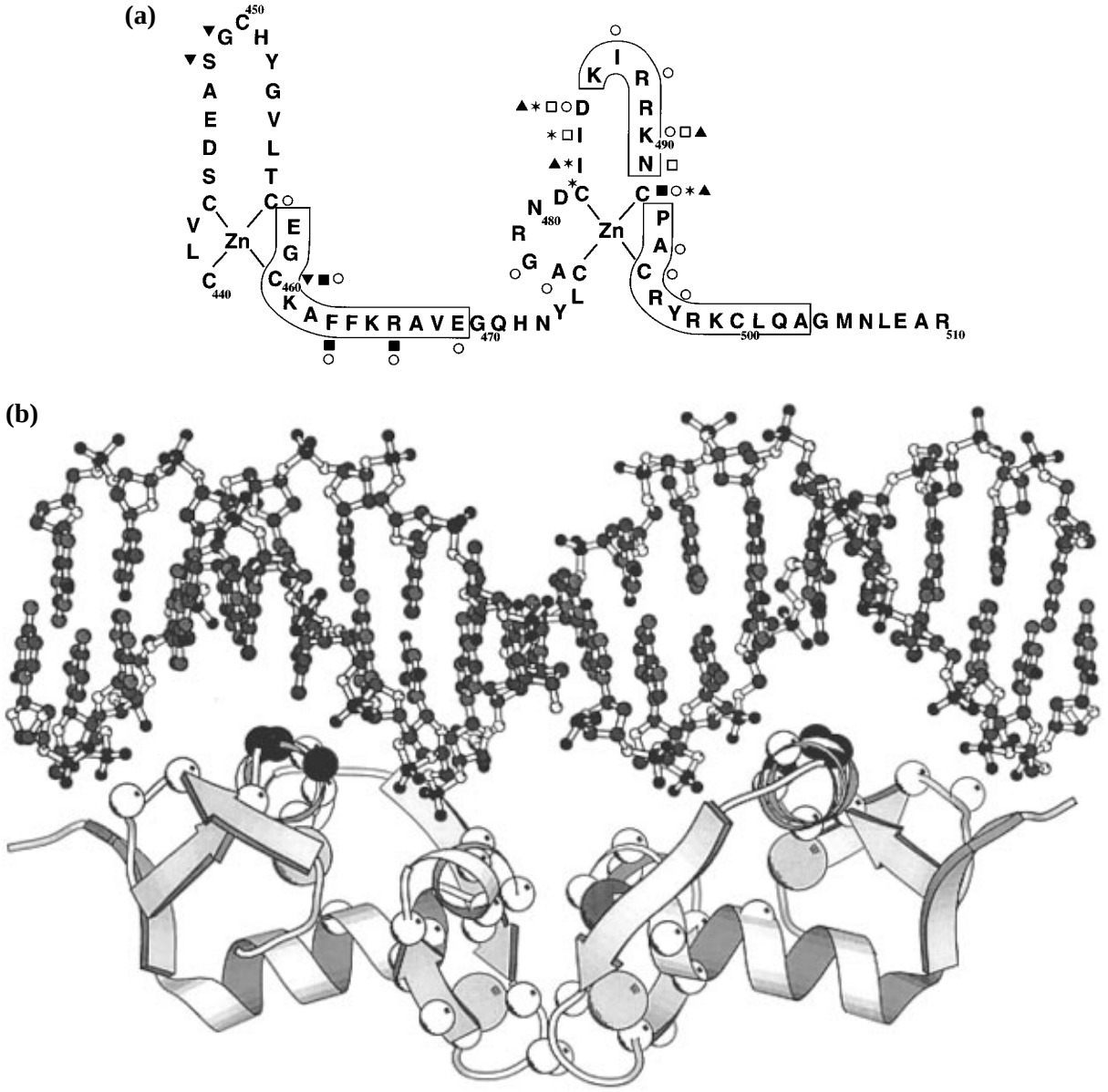


FIGURE 9: (a) Residues that exhibit differences in NMR parameters upon mutation mapped onto the amino acid sequence of $GRDBD_{EGA}$. ■, □, and ○ indicate significant chemical shift differences in the backbone nitrogen, α-proton, and amide proton, respectively. The ∗'s indicate that the amide resonance is broadened in NMR spectra of the mutant. Arrows indicate increased (▲) or decreased (▼) amide proton exchange rates in the mutated protein. (b) Residues that exhibit differences in NMR parameters upon mutation mapped on the crystal structure of the GRDBD−GRE complex (Luisi et al., 1991). The mutated residues are shown as black spheres while the affected residues are shown as white spheres.

sibly discriminate between the two suggested mechanisms for enhanced DNA-binding cooperativity in the mutant. Future studies will reveal what role this structural flexibility plays in sequence specific DNA-binding of these proteins.

## CONCLUDING REMARKS

We have compared several NMR parameters reflecting the solution structures and dynamics of the wild type GRDBD and a triple mutant ($GRDBD_{EGA}$). The investigations were prompted by the observation that the two proteins bind to their high-affinity binding sites on DNA (the GRE and ERE sequences, respectively) with significantly different binding cooperativities (Lundbäck et al., 1994). This effect was somewhat unexpected since the site of the mutation is within the recognition helix where sequence discrimination is thought to occur and is rather distant from the dimerization surface of the GRDBD. The initial observation might be attributed to either one of the following two scenarios: (a) differences in the structure or dynamics of the free proteins, possibly in combination with a different extent of conformational change upon binding to DNA, or (b) as a result of different binding modes (orientations) in the bound states. Although the present investigation does not allow us to discriminate between these mechanisms, it provides clear evidence for a difference in dynamics and/or local stability of the dimerization region in the uncomplexed state of the mutant protein. The structural basis for the differences between the wild type and mutant proteins is likely to be a consequence of the disruption of a hydrogen bond network which links (wild type) S459 in the recognition helix to the second zinc-coordinating domain, where a decreased local stability is observed. Finally, we note that several structural studies of the related ERDBD which, like $GRDBD_{EGA}$, recognizes an ERE binding site suggest that the second zinc-coordinating domain of this protein is disordered in the uncomplexed state (Schwabe et al., 1990) and may adopt

different conformations in the complexed state (Schwabe et al., 1993, 1995).

## ACKNOWLEDGMENT

We thank Dr. Johanna Zilliacus, Karolinska Institutet, for providing an overexpression plasmid for $GRDBD_{EGA}$.

## REFERENCES

Bai, Y., Milne, J. S., Mayne, L., & Englander, S. W. (1993) *Proteins: Struct., Funct., Genet. 17*, 75−86.

Baumann, H., Paulsen, K., Kovács, H., Berglund, H., Wright, A. P. H., Gustafsson, J.-Å., & Härd, T. (1993) *Biochemistry 32*, 13463−13471.

Berglund , H., Kovács, H., Dahlman-Wright, K., Gustafsson, J.-Å., & Härd, T. (1992) *Biochemistry 31*, 12001−12011.

Dahlman-Wright, K., Siltala-Roos, H., Carlstedt-Duke, J., & Gustafsson, J.-Å. (1990) *J. Biol. Chem. 265*, 1430−1435.

Dahlman-Wright, K., Wright, A., Gustafsson, J.-Å., & Carlstedt-Duke, J. (1991) *J. Biol. Chem. 266*, 3107−3112.

Danielsen, M., Hinck, L., & Ringold, G. M. (1989) *Cell 57*, 1131−1138.

Davis, A. L., Keeler, J., Laue, R. D., & Moskau, D. (1992) *J. Magn. Reson. 98*, 207−216.

Englander, S. W., & Kallenbach, N. R. (1984) *Q. Rev. Biophys. 16*, 521−655.

Forsén, S., & Hoffman, R. A. (1963) *J. Chem. Phys. 39*, 2892−2901.

Freedman, L. P., Luisi, B. F., Korszun, Z. R., Basavappa, R., Sigler, P. B., & Yamamoto, K. R. (1988) *Nature 334*, 543−546.

Gewirth, D. T., & Sigler, P. B. (1995) *Nat. Struct. Biol. 2*, 386−394.

Griesinger, C., Otting, G., Wüthrich, K., & Ernst, R. R. (1988) *J. Am. Chem. Soc. 110*, 7870−7872.

Gronenborn, A. M., Ad, B., Wingfield, P. T., & Clore, G. M. (1989) *FEBS Lett. 243*, 93−98.

Gryk, M. R., Finucane, M. D., Zheng, Z., & Jardetzky, O. (1995) *J. Mol. Biol 246*, 618−627.

Härd, T., Kellenbach, E., Boelens, R., Maler, B. A., Dahlman, K., Freedman, L. P., Carlstedt-Duke, J., Yamamoto, K. R., Gustafsson, J.-Å., & Kaptein, R. (1990) *Science 249*, 157−160.

Hvidt, A., & Nielsen, S. O. (1966) *Adv. Protein Chem. 21*, 287−368.

Kraulis, P. J. (1989) *J. Magn. Reson. 24*, 627−633.

Kraulis, P. J. (1991) *J. Appl. Crystallogr. 24*, 946−950.

Kuboniwa, H., Grzesiek, S., Delaglio, F., & Bax, A. (1994) *J. Biomol. NMR 4*, 871−878.

Luisi, B. F., Xu, W. X., Otwinowski, Z., Freedman, L. P., Yamamoto, K. R., & Sigler, P. B. (1991) *Nature 352*, 497−505.

Lundbäck, T., Zilliacus, J., Gustafsson, J.-Å., Carlstedt-Duke, J., & Härd, T. (1994) *Biochemistry 33*, 5955−5965.

Macura, A., & Ernst, R. R. (1980) *Mol. Phys. 41*, 95−117.

Mader, S., Kumar, V., de Verneuil, H., & Chambon, P. (1989) *Nature 338*, 271−274.

Peng, J. W., & Wagner, G. (1992) *J. Magn. Reson. 98*, 308−332.

Schwabe, J. W., Chapman, L., & Rhodes, D. (1995) *Structure 3*, 201−213.

Schwabe, J. W. R., Neuhaus, D., & Rhodes, D. (1990) *Nature 348*, 458−461.

Schwabe, J. W. R., Chapman, L., Finch, J. T., & Rhodes, D. (1993) *Cell 75*, 567−578.

Spera, S., Ikura, M., & Bax, A. (1991) *J. Biol. NMR 1*, 155−165.

Umesono, K., & Evans, R. M. (1989) *Cell 57*, 1139−1146.

van Tilborg, M. A. A., Bonvin, A. M. J. J., Hård, K., Davis, A. L., Maler, B., Boelens, R., Yamamoto, K. R., & Kaptein, R. (1995) *J. Mol. Biol. 247*, 689−700.

Xu, W., Alroy, I., Freedman, L. F., & Sigler, P. B. (1993) *Cold Spring Harbor Symp. Quant. Biol. 58*, 133−139.

Zhao, D., Arrowsmith, C. H., Jia, X., & Jardetzky, O. (1993) *J. Mol. Biol. 229*, 735−746.

Zheng, Z., Czaplicki, J., & Jardetzky, O. (1995) *Biochemistry 34*, 5212−5223.

Zilliacus, J., Dahlman-Wright, K., Wright, A., Gustafsson, J.-Å., & Carlstedt-Duke, J. (1991) *J. Biol. Chem. 266*, 3101−3106.

Zilliacus, J., Wright, A. P. H., Norinder, U., Gustafsson, J.-Å., & Carlstedt-Duke, J. (1992) *J. Biol. Chem. 267*, 24941−24947.

Zilliacus, J., Carlstedt-Duke, J., Gustafsson, J.-Å., & Wright, A. P. H. (1994) *Proc. Natl. Acad. Sci. U.S.A. 91*, 4175−4179.

BI970343I